International Journal of Heat and Mass Transfer 131 (2019) 815–821

Contents lists available at ScienceDirect

International Journal of Heat and Mass Transfer

journal homepage: www.elsevier.com/locate/ijhmt

A simple model for puffing/micro-explosions in water-fuel emulsion droplets

S.S. Sazhin [a,*], O. Rybdylova [a], C. Crua [a], M. Heikal [a,b], M.A. Ismael [b], Z. Nissar [b], A. Rashid B.A. Aziz [b]

[a] Sir Harry Ricardo Laboratories, Advanced Engineering Centre, School of Computing, Engineering and Mathematics, University of Brighton, Brighton BN2 4GJ, UK
[b] Center for Automotive Research and Electric Mobility (CAREM), Universiti Teknologi PETRONAS, 32610 Seri Iskandar, Perak, Malaysia

ARTICLE INFO

Article history:
Received 3 August 2018
Received in revised form 26 October 2018
Accepted 13 November 2018

Keywords:
n-Dodecane
Droplets
Micro-explosions
Puffing
Heat conduction equation

ABSTRACT

A new simple model for the puffing/micro-explosion of water-fuel emulsion droplets is suggested. The model is based on the assumption that a spherical water sub-droplet is located in the centre of a larger fuel droplet. The fuel is approximated by n-dodecane. The fuel droplet surface temperature is assumed to be fixed, and fuel evaporation is ignored. The heat conduction equation is solved inside this composite droplet with the Dirichlet boundary condition at the surface of the fuel droplet. The time instant when the temperature at the interface between water and fuel reaches the boiling temperature of water is associated with the start of the puffing process leading to micro-explosion. This time is referred to as the time to puffing, or micro-explosion delay time. When the fuel surface temperature is equal to the boiling temperature of fuel then this time is expected to be the shortest of the possible times. The predictions of the model are shown to be in agreement with available experimental data. The model predicts an increase in this time with increase in the fuel droplet size for fixed water and fuel mass fractions, in agreement with observations.
© 2018 The Authors. Published by Elsevier Ltd. This is an open access article under the CC BY-NC-ND license (http://creativecommons.org/licenses/by-nc-nd/4.0/).

1. Introduction

The potential for water-in-diesel emulsions to simultaneously reduce NOx and particulate emissions has generated significant attention. Water-emulsified fuels could be an efficient approach to the reduction of exhaust emissions while improving engine performance, without requiring any engine modification. Diesel and biodiesel-Diesel emulsions were found to increase brake thermal efficiency by approximately 6%, with a 30% reduction in NOx and smoke, and a 70% reduction in unburnt hydrocarbons [1]. An increase in brake specific fuel consumption (BSFC) is obtained due to the lower calorific value of the emulsions [2] as water displaces fuel. The increase in water concentration results in longer ignition delays due to the lower volatility and higher viscosity of water [3]. The reduction in NOx seems to be related to reduction of in-cylinder temperature obtained through the evaporation of the emulsion's water [4,5]. The increased formation of hydroxyl radicals reduces soot emissions by increasing the oxidization rate [6]. Research shows that the properties of the dispersed water droplets significantly affect NOx emissions [7] and engine efficiency [8], with smaller dispersed droplet sizes leading to improvements in combustion and emissions. There is also some indication that the combustion process is improved through an increased secondary atomization [9,10], leading to better air-fuel mixing [11]. It is important to note that the fuel injection hardware can significantly affect the emulsion properties, with the dispersed droplet sizes reducing significantly after the emulsion is compressed by the high-pressure fuel pump, and again after being injected through the nozzle orifices [12].

A widely used mechanism to improve fuel mixing is through the phenomena of puffing and micro-explosion in emulsion droplets, which could promote the secondary atomization process through a rapid break-up of the parent droplets due to the different volatility of the fuel (continuous phase) and water (dispersed phase). Puffing is the partial ejection of some of the dispersed water out of an emulsion droplet [14], while micro-explosion is the complete break-up of the parent droplet. The roles of puffing and micro-explosions in water-in-fuel emulsion droplets in internal combustion engines have been widely discussed in the literature (e.g. [13–16] and the references therein). Both phenomena enhance the effective fuel droplet size distribution, air-fuel mixing, and ultimately fuel efficiency [17]. Observations show that these events are influenced by water concentration, surfactant type, and dispersed water droplet size and temperature [18,19]. Some researchers observed that the intensity of micro-explosions

* Corresponding author.
E-mail address: S.Sazhin@brighton.ac.uk (S.S. Sazhin).

https://doi.org/10.1016/j.ijheatmasstransfer.2018.11.065
0017-9310/© 2018 The Authors. Published by Elsevier Ltd.
This is an open access article under the CC BY-NC-ND license (http://creativecommons.org/licenses/by-nc-nd/4.0/).

Nomenclature

a	$1/\sqrt{\kappa}$
A	function introduced in Solution (A1.8)
b	weight of functions $v_n(R)$ (J/(m^3 K))
B	function introduced in Solution (A1.8)
c	specific heat capacity (J/(kg K))
h	convective heat transfer coefficient (W/(m^2 K))
k	thermal conductivity (W/(m K))
P	radiation source term in Eq. (1) (K/s)
$p_n(t)$	functions introduced in Eq. (8) (K m/s)
R	distance from the droplet centre (m)
$R_{w(d)}$	radius of the water sub-droplet (droplet) (m)
t	time (s)
T	temperature (K)
T_0	$T_s - T_{d0}$ (K)
u	$(T - T_s)R$
v_n	eigenfunctions found from Eq. (12)
$\|\|v_n\|\|^2$	norm of v_n with weight b (J/(m^2 K))

Greek symbols

$\Theta_n(t)$	function introduced in Eq. (A1.4) (K m)
$\Theta_{n1}(t)$	function defined by Eq. (9) (K m)
$\Theta_{n2}(t)$	function defined by Eq. (10) (K m)
κ	thermal diffusivity (m^2/s)
λ_n	eigenvalues found from Eq. (13) ($1/\sqrt{s}$)
ρ	density (kg/m^3)

Subscripts

d	droplet
f	fuel (n-dodecane)
g	ambient gas
s	surface
w	water
0	initial conditions

increased with water content [20,21] as well as with the droplet size of the dispersed water phase.

It seems that Ivanov and Nefedov [22] were the first to draw attention to micro-explosions as a mechanism for accelerated evaporation of emulsion fuel droplets where water was the volatile component. Since this pioneering paper a number of models for micro-explosions have been suggested, starting with relatively simple ones [23,24] and ending with the recently suggested most advanced models [14–16].

Although the models developed in [14–16] are undoubtedly very useful for understanding the physical background of the processes involved in puffing/micro-explosions in droplets, the usefulness of these models for engineering applications is less obvious. Engineers dealing with puffing/micro-explosions are interested primarily in the integral characteristics of the process, such as the puffing/micro-explosion delay times, rather than in the details of the processes inside the deforming and exploding droplet. In our paper, the results of the development of a simple model specifically focused on the prediction of these delay times are presented and discussed.

2. Description of the new model

The model is based on the assumption that a spherical water sub-droplet is located in the centre of a fuel droplet as shown in Fig. 1. In this figure, R_w and R_d are the radii of the water sub-droplet and fuel droplet, respectively. T_w and T_s in this figure are the temperature at the interface between water and fuel and the temperature at the surface of the fuel droplet, respectively. The fuel is approximated by n-dodecane. The temperature T_s is assumed to be fixed, and fuel evaporation is ignored. The droplet is assumed to be stationary and penetration of heat from the surface of the droplet to its interior is described by a one-dimensional transient heat conduction equation. This equation is solved analytically inside this composite droplet with the Dirichlet boundary condition at its surface, and the solution leads to a time-dependent distribution of temperature inside the droplet. If T_s is greater than the initial temperature inside the droplet, assumed to be homogeneous, then the temperature between the centre of the droplet and its surface will increase. If T_s is greater than the boiling temperature of water, at a certain time instant T_w is expected to reach this boiling temperature. This time instant is associated with the start of the puffing process leading to micro-explosion. This time is referred to as the time to puffing, or micro-explosion delay time. The maximal value of T_s is assumed to be equal to the boiling temperature of n-dodecane. In this case, the micro-explosion delay time is expected to be minimal.

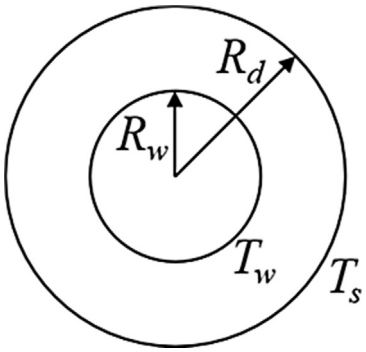

Fig. 1. Diagram showing the location of a water sub-droplet of radius R_w inside the fuel (n-dodecane) droplet of radius R_d. T_w is the temperature at the interface between water and fuel, T_s is the droplet surface temperature.

Note that a number of authors drew attention to the fact that the start of the puffing processes can be associated with the time instant when T_w reaches the nucleation rather than boiling temperature [25]. The former temperature is defined as the mean temperature in the range in which the nucleation rate changes from a negligible value to a very large value [25]. We have not, however, found reliable values of this temperature for the conditions of the experiment which will be used for validation of our model. To be consistent with our other simplifying assumptions of the model we base our analysis on the assumption that puffing starts at the boiling temperature.

The mathematical details of the model are described in the next section. The results of the application of the model to the analysis of experimentally observed puffing/micro-explosions in composite water-n-dodecane droplets are described in Section 4. The main results of the paper are summarised in Section 5.

3. Basic equations and approximations

The variation of the temperature in the water-fuel domain, shown in Fig. 1, is described by the heat conduction equation in the form [26,27]:

$$\frac{\partial T}{\partial t}=\kappa\left(\frac{\partial^2 T}{\partial R^2}+\frac{2}{R}\frac{\partial T}{\partial R}\right)+P(t,R), \tag{1}$$

where

$$\kappa=\begin{cases}\kappa_w=k_w/(c_w\rho_w) & \text{when} \quad R\leqslant R_w\\ \kappa_f=k_f/(c_f\rho_f) & \text{when} \quad R_w<R\leqslant R_d,\end{cases} \tag{2}$$

$\kappa_{w(f)}$ is the water (liquid fuel) thermal diffusivity, $k_{w(f)}$ is the water (liquid fuel) thermal conductivity, $c_{w(f)}$ is the water (liquid fuel) specific heat capacity, $\rho_{w(f)}$ is the water (liquid fuel) density, R is the distance from the centre of the droplet, t is time. The source term $P(t,R)$ takes into account the volumetric droplet heating (e.g. heating due to thermal radiation).

Eq. (1) needs to be solved subject to initial and boundary conditions:

$$T|_{t=0}=\begin{cases}T_{w0}(R) & \text{when} \quad R\leqslant R_w\\ T_{f0}(R) & \text{when} \quad R_w<R\leqslant R_d,\end{cases} \tag{3}$$

$$T|_{R=R_w^-}=T|_{R=R_w^+}, \quad k_w\frac{\partial T}{\partial R}\bigg|_{R=R_w^-}=k_f\frac{\partial T}{\partial R}\bigg|_{R=R_w^+}, \tag{4}$$

$$h\left(T_g-T(R_d)\right)=k_f\frac{\partial T}{\partial R}\bigg|_{R=R_d-0}, \tag{5}$$

where h is the convection heat transfer coefficient, describing the heating of the droplet. To ensure consistency between Conditions (3) and (4) we assume that $T_{w0}(R_w)=T_{f0}(R_w)$.

Expression (5) is the well-known Robin boundary condition widely used for the analysis of droplet heating and evaporation [28]. Let us rewrite this equation as:

$$T(R_d)\equiv T_s=T_g-\frac{k_f}{h}\frac{\partial T}{\partial R}\bigg|_{R=R_d-0}. \tag{6}$$

If the solution to Eq. (1) is performed at a small time step, we could make an assumption that $T_g=T_{g0}=\text{const}$ and $h=\text{const}$. Moreover, we could take the value of $\frac{\partial T}{\partial R}|_{R=R_d-0}$ in (6) from the initial condition for the first time step and from the results of calculation for the previous time steps for all the following steps. This would allow us to assume that the right hand side of Eq. (6) is constant and reduce the Robin boundary condition (5) to the Dirichlet boundary condition:

$$T(R_d)\equiv T_s. \tag{7}$$

To be consistent with the previous simplifying assumptions of the model, we will make several further simplifying assumptions.

1. The temperature of the droplet surface is assumed to be constant during the whole period of droplet heating (not just during individual time steps). This would have been a natural assumption for the times after the droplet surface temperature reaches the boiling point. In the general case, the assumption that the droplet surface temperature is equal to the boiling temperature of the liquid fuel would allow us to predict the minimal time to puffing and micro-explosion delay time. More realistic values of this temperature are expected to be below the liquid fuel boiling temperature and this will be taken into account in the analysis of our results.
2. The effects of droplet evaporation and swelling are ignored. This means that we assume that puffing/micro-explosion occurs before the droplet evaporation becomes significant, which is consistent with experimental observations. The effects of swelling are anticipated to be small and can be safely ignored in the analysis remembering the crudeness of the whole model.
3. We assume that both T_{w0} and T_{f0} do not depend on R. Eventually they will be assumed equal to T_{d0}.
4. The effect of the source term (thermal radiation) is taken into account when deriving the formulae, but eventually it will be ignored in our analysis. This approach would allow us to generalise the model in the future to the case where the contribution of thermal radiation is expected to be significant.
5. All thermodynamic and transport properties (liquid thermal conductivities, heat capacities and densities) are taken at the initial droplet temperature. These properties are expected to be relatively weak functions of temperature; ignoring this dependence is considered to be consistent with other simplifying assumptions of the model.

These assumptions allow us to generalise the analysis previously described in [29,30] and derive the analytical solution to Eq. (1), subject to initial and boundary conditions (3), (4) and (7) in the form (see Appendix A for further details):

$$T(R,t)=T_s+\frac{1}{R}\sum_{n=1}^{\infty}\Big[\exp\left(-\lambda_n^2 t\right)(\Theta_{n1}+\Theta_{n2})+\int_0^t\exp\left(-\lambda_n^2(t-\tau)\right)p_n(\tau)\mathrm{d}\tau\Big]v_n(R), \tag{8}$$

where

$$\Theta_{n1}=\frac{T_0 c_w\rho_w}{||v_n||^2(\lambda_n a_w)^2}\left[\lambda_n a_w R_w\cot\left(\lambda_n a_w R_w\right)-1\right], \tag{9}$$

$$\Theta_{n2}=\frac{T_0 c_f\rho_f}{||v_n||^2\left(\lambda_n a_f\right)^2}\left[\lambda_n a_f R_w\cot\left(\lambda_n a_f(R_d-R_w)\right)-\frac{\lambda_n a_f R_d}{\sin\left(\lambda_n a_f(R_d-R_w)\right)}+1\right], \tag{10}$$

$$T_0=T_s-T_{w0}=T_s-T_{f0}, \tag{11}$$

$$v_n(R)=\begin{cases}\pm\frac{\sin(\lambda_n a_w R)}{\sin(\lambda_n a_w R_w)} & \text{when} \quad R<R_w\\ \pm\frac{\sin(\lambda_n a_f(R-R_d))}{\sin(\lambda_n a_f(R_w-R_d))} & \text{when} \quad R_w\leqslant R\leqslant R_d,\end{cases} \tag{12}$$

$$||v_n||^2=\frac{c_w\rho_w R_w}{2\sin^2(\lambda_n a_w R_w)}+\frac{c_f\rho_f(R_d-R_w)}{2\sin^2(\lambda_n a_f(R_w-R_d))}-\frac{k_w-k_f}{2R_w\lambda_n^2},$$

$$p_n(t)=\frac{c_w\rho_w}{||v_n||^2}\int_0^{R_w}RP(t,R)v_n(R)\mathrm{d}R+\frac{c_f\rho_f}{||v_n||^2}\int_{R_w}^{R_d}RP(t,R)v_n(R)\mathrm{d}R.$$

A countable set of positive eigenvalues λ_n is found from the solution to the equation:

$$\sqrt{k_w c_w\rho_w}\cot(\lambda a_w R_w)-\sqrt{k_f c_f\rho_f}\cot(\lambda a_f(R_w-R_d))=\frac{k_w-k_f}{R_w\lambda}. \tag{13}$$

These are arranged in ascending order $0<\lambda_1<\lambda_2<\ldots..$ $a_w=\sqrt{\frac{c_w\rho_w}{k_w}}$, $a_f=\sqrt{\frac{c_f\rho_f}{k_f}}$.

In Expression (12) sign '−' was chosen in order to obtain a physically meaningful solution when $T\leqslant T_s$.

4. Analysis

Experiments were conducted in a heated vessel (700 K) at atmospheric pressure, with optical access to observe the sprayed emulsion. The experimental setup is described in [31]. The time

to puffing was measured using a high-speed camera fitted with a long-distance microscope, the images from which were processed to measure the initial droplet diameters and the time to puffing. In order to account for the significant effects of the fuel injection system on the properties of the dispersed phase [12], we first ran the emulsion through a high-pressure pump and injector. This enabled us to collect and analyse the sprayed samples' dispersed water droplets before injecting the emulsion into the optical vessel using a low-pressure micro-syringe.

The experiments were performed with a resolution of 256×800 pixels^2, frame rate of 12,000 frames per second, and exposure time of 2 μs. The image scale factor was 0.0185 mm/pixel. Hence, the uncertainty for the time to puffing was linked to the identification of the frames for droplet creation and start of puffing, which corresponds to ±167 μs. The uncertainty for the measurement of the droplet diameter was related to the detection of the droplet perimeter, which is estimated to be ±37 μm. Droplets with diameters smaller than 50 μm were ignored due to the large experimental uncertainty.

We considered typical initial values of parameters for n-dodecane droplets with the water sub-droplets inside them, droplet surface temperatures and ambient gas parameters listed in Table 1. Having substituted these values into Eq. (8) we found the distribution of temperature inside droplets at various time instants. An example of such distributions for a droplet of radius 25 μm, initial homogeneous temperature inside the droplet equal to 434 K and droplet surface temperature equal to 489.47 K (boiling temperature of n-dodecane) is shown in Fig. 2. In this figure, the values of temperature inside droplets are shown as the functions of the distance from the droplet centre (R) normalised by the radius of the water sub-droplet (R_w). For the chosen values of input parameters, for the surface of the droplet $R_d/R_w = 1.88$. The curves 1, 2, 3, 4 and 5 refer to time instants 1.1 μs, 11 μs, 0.11 ms, 0.25 ms and 0.5 ms, respectively. As follows from this figure, for curve 5, corresponding to time instant 0.5 ms, the predicted temperature at $R = R_w$ is very close to 373.15 K, which is the boiling temperature of water. We anticipate that at this time instant evaporation of water will lead to puffing above the surface of the water sub-droplet eventually leading to micro-explosion. This time instant is commonly known as time to puffing. We assume that the micro-explosion takes place shortly after the start of puffing.

Plots similar to those presented in Fig. 2 were prepared for all droplet radii, and initial and surface droplet temperatures shown in Table 1. For all these plots, the values of time to puffing were obtained. The values of these times are shown in Fig. 3 as functions of droplet diameters for various initial and surface droplet temperatures. In the same figure the experimentally observed times to puffing for various droplet diameters are shown.

As can be seen from Fig. 3, the values of predicted times to puffing for droplet surface temperature equal to the boiling temperature of n-dodecane are always less than those observed experimentally. In most cases, the orders of magnitude of the predicted times to puffing for other values of droplet surface

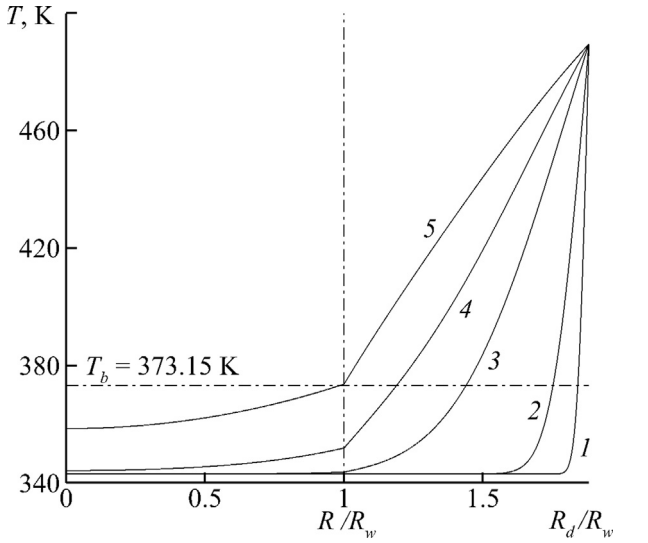

Fig. 2. The plots predicted by the new model of temperatures inside the composite droplet (T) versus normalised distance from the droplet centre R/R_w at 5 instants of time: 1.1 μs (curve 1), 11 μs (curve 2), 0.11 ms (curve 3), 0.25 ms (curve 4) and 0.5 ms (curve 5).

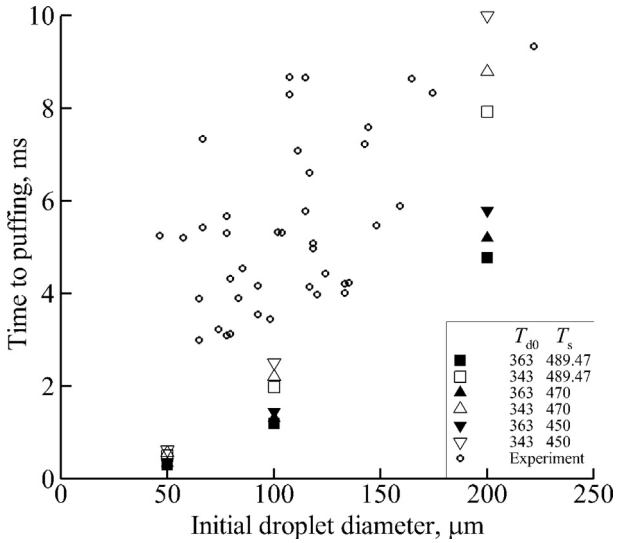

Fig. 3. The values of time to puffing, predicted by the new model, versus the initial droplet diameters for two values of the initial droplet temperature and three values of droplet surface temperature (see the insert in this figure). The experimentally observed values of this time are shown as empty circles.

Table 1
Droplet and gas properties.

Parameter	Value
Parent droplet radii (R_d) [μm]	25; 50; 100
Droplet initial composition [vol]	0.15 water + 0.85 n-dodecane
n-dodecane density (ρ_f) [kg/m^3]	825
Gas composition	air
Droplet surface temperatures (T_s) [K]	489.47 (boiling temperature), 470, 450
Initial droplet temperature (T_{d0}) [K]	343 and 363
Gas (air) pressure [MPa]	0.1

temperature are the same as those observed experimentally. This does not apply to the results for small droplets with diameters equal to 50 μm for which only one experimental result is available. The predicted increase in times to puffing with the increase in the initial droplet diameters is confirmed by experimental observations, despite considerable scatter of experimental data. The model, however, cannot explain noticeably shorter times to puffing for smaller droplets (with diameters less than 100 μm) than observed experimentally. This could be partly explained by the fact that we linked the start of puffing with the time instant when the water sub-droplet temperature reached the boiling rather than nucleation temperature.

The decrease in the surface temperature leads to an increase in the time to puffing, as expected, although this result cannot be confirmed experimentally at this stage. These results allow us to conclude that the suggested new model, despite its simplicity, is

able to describe the processes leading to puffing and micro-explosions, not only qualitatively but also quantitatively at least in some cases.

5. Conclusions

A new model for puffing/micro-explosions in water-fuel emulsion droplets is suggested. The model is based on the assumption that a spherical water sub-droplet is located in the centre of a stationary fuel droplet. The fuel is approximated by n-dodecane, the droplet surface temperature is assumed to be fixed, and fuel evaporation is ignored. The penetration of heat from the surface of the droplet to its interior is described by a one-dimensional transient heat conduction equation. This equation is solved analytically inside the composite droplet with the Dirichlet boundary condition at its surface, and the solution leads to a time-dependent distribution of temperature inside the droplet. If the droplet surface temperature is greater than the boiling temperature of water, at a certain time instant the temperature at the interface between water and fuel is expected to reach this boiling temperature. This time instant is referred to as the time to puffing, or micro-explosion delay time.

It is shown that the values of predicted times to puffing for droplet surface temperature equal to the boiling temperature of n-dodecane are always less than those observed experimentally, as expected. The predicted increase in these times with an increase in the initial droplet diameters is also confirmed by experimental observations. These results allow us to conclude that, despite its simplicity, the suggested model is able to describe the processes leading to puffing and micro-explosions not only qualitatively but also in some cases quantitatively.

The models which we developed can be easily generalised to modelling puffing/micro-explosion processes in other composite droplets. Moreover, the equations which we derived, could be applied to the analysis of the processes leading to puffing/micro-explosion in the presence of thermal radiation.

Conflict of interets

None.

Acknowledgements

The current work was carried out as a collaboration between The University of Brighton, supported by the EPSRC, UK (Grants EP/M002608/1 and EP/R012024/1), and the Centre for Automotive Research and Electric Mobility (CAREM), the Universiti Teknologi PETRONAS (UTP), supported by the ministry of higher education Fundamental Research Grant Scheme (FRGS) (Grant FRGS/1/2017/TK10/UTP/01/2) and UTP Graduate Assistant (GA) studentship.

Appendix A. Derivation of Formula (8)

Introducing a new variable

$$u = (T - T_s)\, R$$

we can simplify Eq. (1) and initial and boundary conditions (3) and (4) to:

$$\frac{\partial u}{\partial t} = \kappa \frac{\partial^2 u}{\partial R^2} + RP(t,R), \tag{A1.1}$$

$$u|_{t=0} = -T_0 R \ \text{ when } \ 0 \leqslant R \leqslant R_d, \tag{A1.2}$$

$$u|_{R=R_w^-} = u|_{R=R_w^+}, \ \ k_w\left[R_w u_R' - u\right]\big|_{R=R_w^-} = k_f\left[R_w u_R' - u\right]\big|_{R=R_w^+}, \ \ u|_{R=R_d} = 0, \tag{A1.3}$$

where $T_0 \equiv T_s - T_{d0}(R)$ does not depend on R in our case. The temperature at the surface of the droplet (T_s) is assumed to be constant.

Conditions (A1.3) need to be amended by the boundary condition at $R = 0$. Since $T - T_s$ is finite at $R = 0$ then $u|_{R=0} = 0$. We look for the solution to Eq. (A1.1) in the form:

$$u = \sum_{n=1}^{\infty} \Theta_n(t)\, v_n(R), \tag{A1.4}$$

where functions $v_n(R)$ form the full set of non-trivial solutions to the eigenvalue problem:

$$\frac{\mathrm{d}^2 v}{\mathrm{d}R^2} + a^2 \lambda^2 v = 0 \tag{A1.5}$$

subject to boundary conditions:

$$\left.\begin{aligned} &v|_{R=0} = v|_{R=R_d} = 0 \\ &v|_{R=R_w^-} = v|_{R=R_w^+} \\ &k_w\left[R_w v_R' - v\right]\big|_{R=R_w^-} = k_f\left[R_w v_R' - v\right]\big|_{R=R_w^+} \end{aligned}\right\}, \tag{A1.6}$$

where

$$a = \frac{1}{\sqrt{\kappa}} = \begin{cases} \sqrt{\frac{c_w \rho_w}{k_w}} \equiv a_w & \text{when} \quad R \leqslant R_w \\ \sqrt{\frac{c_f \rho_f}{k_f}} \equiv a_f & \text{when} \quad R_w < R \leqslant R_d. \end{cases} \tag{A1.7}$$

Note that λ has dimension $1/\sqrt{\text{time}}$. We look for the solution to Eq. (A1.5) in the form:

$$v(R) = \begin{cases} A \sin(\lambda a_w R) & \text{when} \quad R \leqslant R_w \\ B \sin(\lambda a_f (R - R_d)) & \text{when} \quad R_w < R \leqslant R_d. \end{cases} \tag{A1.8}$$

Function (A1.8) satisfies boundary conditions (A1.6) at $R = 0$. Having substituted function (A1.8) into boundary conditions (A1.6) at $R = R_w$ we obtain:

$$A \sin(\lambda a_w R_w) = B \sin(\lambda a_f (R_w - R_d)), \tag{A1.9}$$

$$\begin{aligned} &Ak_w[R_w \lambda a_w \cos(\lambda a_w R_w) - \sin(\lambda a_w R_w)] \\ &\quad = Bk_f\left[R_w \lambda a_f \cos(\lambda a_f (R_w - R_d)) - \sin(\lambda a_f (R_w - R_d))\right]. \end{aligned} \tag{A1.10}$$

Condition (A1.9) is satisfied when:

$$\left.\begin{aligned} A &= \pm[\sin(\lambda a_w R_w)]^{-1} \\ B &= \pm\left[\sin(\lambda a_f (R_w - R_d))\right]^{-1} \end{aligned}\right\}. \tag{A1.11}$$

The sign in Eq. (A1.11) can be chosen to ensure that u in Eq. (A1.4) is negative. Note that we need to choose either '+' or '−' in both expressions.

Having substituted Eq. (A1.11) into (A1.10) we obtain:

$$k_w[R_w \lambda a_w \cot(\lambda a_w R_w) - 1] = k_f\left[R_w \lambda a_f \cot(\lambda a_f (R_w - R_f)) - 1\right]. \tag{A1.12}$$

Remembering the definitions of a_w and a_f, Eq. (A1.12) can be simplified to:

$$\begin{aligned} &\sqrt{k_w c_w \rho_w}\cot(\lambda a_w R_w) - \sqrt{k_f c_f \rho_f}\cot(\lambda a_f (R_w - R_d)) \\ &\quad = \frac{k_w - k_f}{R_w \lambda}. \end{aligned} \tag{A1.13}$$

Eq. (A1.13) allows us to find a countable set of positive eigenvalues λ_n [26] which can be arranged in ascending order $0 < \lambda_1 < \lambda_2 < \ldots$. Note that the negative solutions $-\lambda_n$ also satisfy Eq. (A1.13) as both sides of this equation are odd functions of λ. $\lambda = 0$, however, does not satisfy this equation. Having substituted these values of λ_n into Eq. (A1.8) and remembering Eq. (A1.11) we obtain the expressions for eigenfunctions v_n in the form:

$$v_n(R)=\begin{cases}\pm\frac{\sin(\lambda_n a_w R)}{\sin(\lambda_n a_w R_w)} & \text{when} \quad R\leqslant R_w\\ \pm\frac{\sin(\lambda_n a_f(R-R_d))}{\sin(\lambda_n a_f(R_w-R_d))} & \text{when} \quad R_w<R\leqslant R_d\end{cases}. \tag{A1.14}$$

It can be shown (see [29]) that functions $v_n(R)$ are orthogonal with weight

$$b=\begin{cases}k_w a_w^2=c_w\rho_w & \text{when} \quad R\leqslant R_w\\ k_f a_f^2=c_f\rho_f & \text{when} \quad R_w<R\leqslant R_d\end{cases}.$$

This means that: $\int_0^{R_g} v_n(R)v_m(R)b\mathrm{d}R=\delta_{nm}||v_n||^2$,where

$$\delta_{nm}=\begin{cases}1 & \text{when} \quad n=m\\ 0 & \text{when} \quad n\neq m\end{cases}.$$

See [29] for the discussion of completeness of this set of functions.

The norm of v_n with weight b is calculated as:

$$\begin{aligned}||v_n||^2&=\int_0^{R_d} v_n^2 b\mathrm{d}R\\ &=\int_0^{R_w}\left[\frac{\sin(\lambda_n a_w R)}{\sin(\lambda_n a_w R_w)}\right]^2 c_w\rho_w\mathrm{d}R\\ &\quad+\int_{R_w}^{R_d}\left[\frac{\sin(\lambda_n a_f(R-R_d))}{\sin(\lambda_n a_f(R_w-R_d))}\right]^2 c_f\rho_f\mathrm{d}R\\ &=\frac{c_w\rho_w}{2\sin^2(\lambda_n a_w R_w)}\left[R_w-\frac{\sin(2\lambda_n a_w R_w)}{2\lambda_n a_w}\right]\\ &\quad+\frac{c_f\rho_f}{2\sin^2(\lambda_n a_f(R_w-R_f))}\left[R_d-R_w+\frac{\sin(2\lambda_n a_w(R_w-R_d))}{2\lambda_n a_g}\right]\\ &=\frac{c_w\rho_w R_w}{2\sin^2(\lambda_n a_w R_w)}+\frac{c_f\rho_f(R_d-R_w)}{2\sin^2(\lambda_n a_f(R_w-R_d))}\\ &\quad-\frac{k_w-k_f}{2R_w\lambda_n^2}.\end{aligned} \tag{A1.15}$$

When deriving Eq. (A1.15) we took into account Eq. (A1.13). Since all functions v_n satisfy boundary conditions (A1.6), function u defined by Expression (A1.4) satisfies boundary conditions (A1.3).

Let us expand $RP(t,R)$ in a series over v_n:

$$RP(t,R)=\sum_{n=1}^{\infty}p_n(t)v_n(R), \tag{A1.16}$$

where:

$$p_n(t)=\frac{1}{||v_n||^2}\int_0^{R_d} RP(t,R)v_n(R)b\mathrm{d}R.$$

Having substituted Eqs. (A1.4) and (A1.16) into Eq. (A1.1) we obtain:

$$\sum_{n=1}^{\infty}\Theta_n'(t)v_n(R)=-\sum_{n=1}^{\infty}\Theta_n(t)\lambda_n^2 v_n(R)+\sum_{n=1}^{\infty}p_n(t)v_n(R). \tag{A1.17}$$

When deriving Eq. (A1.17) we took into account that functions $v_n(R)$ satisfy Eq. (A1.5) for $\lambda=\lambda_n$. Eq. (A1.17) is satisfied if and only if:

$$\Theta_n'(t)=-\lambda_n^2\Theta_n(t)+p_n(t). \tag{A1.18}$$

The initial condition for $\Theta_n(t)$ can be obtained after substituting Expression (A1.4) into initial condition (A1.2) for u:

$$\sum_{n=1}^{\infty}\Theta_n(0)v_n(R)=-T_0R \quad \text{when} \quad 0\leqslant R\leqslant R_d$$

Remembering the orthogonality of v_n with weight b, we obtain from Equation (A1.19):

$$\Theta_n(0)=\frac{1}{||v_n||^2}\int_0^{R_d}(-T_0R)v_n(R)b\mathrm{d}R$$

Remembering that T_0 is constant then this equation can be further simplified to:

$$\Theta_n(0)=\Theta_{n1}+\Theta_{n2} \tag{A1.20}$$

where

$$\Theta_{n1}=\frac{T_0c_w\rho_w}{||v_n||^2(\lambda_n a_w)^2}[\lambda_n a_w R_w\cot(\lambda_n a_w R_w)-1],$$

$$\Theta_{n2}=\frac{T_0c_f\rho_f}{||v_n||^2(\lambda_n a_f)^2}\left[\lambda_n a_f R_w\cot\left(\lambda_n a_f(R_d-R_w)\right)-\frac{\lambda_n a_f R_d}{\sin\left(\lambda_n a_f(R_d-R_w)\right)}+1\right],$$

where $T_0=T_s-T_{w0}=T_s-T_{f0}$.

The solution to Eq. (A1.18) subject to the initial condition (A1.20) can be written as:

$$\Theta_n(t)=\exp\left(-\lambda_n^2 t\right)\Theta_n(0)+\int_0^t\exp\left(-\lambda_n^2(t-\tau)\right)p_n(\tau)\mathrm{d}\tau. \tag{A1.21}$$

Eq. (8) follows from the definition of u and Eqs. (A1.4) and (A1.21).

References

[1] O.A. Elsanusi, M.M. Roy, M.S. Sidhu, Experimental investigation on a Diesel engine fueled by Diesel-biodiesel blends and their emulsions at various engine operating conditions, Appl. Energy 203 (2017) 582–593, https://doi.org/10.1016/j.apenergy.2017.06.052.

[2] J.K. Mwangi, W.-J. Lee, Y.-C. Chang, C.-Y. Chen, L.-C. Wang, An overview: energy saving and pollution reduction by using green fuel blends in diesel engines, Appl. Energy 159 (2015) 214–236, https://doi.org/10.1016/j.apenergy.2015.08.084.

[3] D. Ogunkoya, S. Li, O.J. Rojas, T. Fang, Performance, combustion, and emissions in a diesel engine operated with fuel-in-water emulsions based on lignin, Appl. Energy 154 (2015) 851–861, https://doi.org/10.1016/j.apenergy.2015.05.036.

[4] Y. Xu, P. Hellier, S. Purton, F. Baganz, N. Ladommatos, Algal biomass and diesel emulsions: an alternative approach for utilizing the energy content of microalgal biomass in diesel engines, Appl. Energy 172 (2016) 80–95, https://doi.org/10.1016/j.apenergy.2016.03.019.

[5] H. Taghavifar, S. Anvari, A. Parvishi, Benchmarking of water injection in a hydrogen-fueled diesel engine to reduce emissions, Int. J. Hydrogen Energy 42 (16) (2017) 11962–11975, https://doi.org/10.1016/j.ijhydene.2017.02.138.

[6] B.K. Debnath, U.K. Saha, N. Sahoo, A comprehensive review on the application of emulsions as an alternative fuel for diesel engines, Renew. Sust. Energy Rev. 42 (2015) 196–211, https://doi.org/10.1016/j.rser.2014.10.023.

[7] C.Y. Lin, L.W. Chen, Comparison of fuel properties and emission characteristics of two- and three-phase emulsions prepared by ultrasonically vibrating and mechanically homogenizing emulsification methods, Fuel 87 (10–11) (2008) 2154–2161, https://doi.org/10.1016/j.fuel.2007.12.017.

[8] A.M.A. Attia, A.R. Kulchitskiy, Influence of the structure of water-in-fuel emulsion on diesel engine performance, Fuel 116 (2014) 703–708, https://doi.org/10.1016/j.fuel.2013.08.057.

[9] D.R. Emberson, B. Ihracska, S. Imran, A. Diez, Optical characterization of Diesel and water emulsion fuel injection sprays using shadowgraphy, Fuel 172 (2016) 253–262, https://doi.org/10.1016/j.fuel.2016.01.015.

[10] Y.-C. Chang, W.-J. Lee, S.-L. Lin, L.-C. Wang, Green energy: water-containing acetone-butanol-ethanol diesel blends fueled in diesel engines, Appl. Energy 109 (2013) 182–191, https://doi.org/10.1016/J.APENERGY.2013.03.086.

[11] S.H. Pourhoseini, R. Esmaeeli, Effect of nanosilver/water-in-kerosene emulsion on NOx reduction and enhancement of thermal characteristics of a liquid fuel burner, Energy Fuels 31 (12) (2017) 14288–14295, https://doi.org/10.1021/acs.energyfuels.

[12] M.A. Ismael, M.R. Heikal, A.R. Aziz, F. Syah, A.E.Z. Zainal, C. Crua, The effect of fuel injection equipment on the dispersed phase of water-in-diesel emulsions, Appl. Energy 222 (2018) 762–771, https://doi.org/10.1016/j.apenergy.2018.03.070.

[13] T. Kadota, H. Yamasaki, Recent advances in the combustion of water fuel emulsion, Prog. Energy Combust. Sci. 28 (2002) 385–404, https://doi.org/10.1016/S0360-1285(02)00005-9.

[14] J. Shinjo, J. Xia, L.C. Ganippa, A. Megaritis, Physics of puffing and microexplosion of emulsion fuel droplets, Phys. Fluids 26 (10) (2014) 103302, https://doi.org/10.1063/1.4897918.

[15] J. Shinjo, J. Xia, A. Megaritis, L.C. Ganippa, R.F. Cracknell, Modeling temperature distribution inside a emulsion fuel droplet under convective heating: a key to predicting microexplosion and puffing, Atom. Sprays 26 (2016) 551–583.

[16] J. Shinjo, J. Xia, Combustion characteristics of a single decane/ethanol emulsion droplet and a droplet group under puffing conditions, Proc. Combust. Inst. 36 (2017) 2513–2521.
[17] T. Daho, G. Vaitilingom, S.K. Ouiminga, B. Piriou, A.S. Zongo, S. Ouoba, J. Koulidiati, Influence of engine load and fuel droplet size on performance of a CI engine fueled with cottonseed oil and its blends with diesel fuel, Appl. Energy 111 (2013) 1046–1053, https://doi.org/10.1016/j.apenergy.2013.05.059.
[18] V. Califano, R. Calabria, P. Massoli, Experimental evaluation of the effect of emulsion stability on micro-explosion phenomena for water-in-oil emulsions, Fuel 117 (2014) 87–94, https://doi.org/10.1016/j.fuel.2013.08.073.
[19] E. Mura, P. Massoli, C. Josset, K. Loubar, J. Bellettre, Study of the micro-explosion temperature of water in oil emulsion droplets during the Leidenfrost effect, Exp. Therm. Fluid Sci. 43 (2012) 63–70, https://doi.org/10.1016/j.expthermflusci.2012.03.027.
[20] I. Jeong, K.-H. Lee, J. Kim, Characteristics of auto-ignition and micro-explosion behavior of a single droplet of water-in-fuel, J. Mech. Sci. Technol. 22 (1) (2008) 148–156, https://doi.org/10.1007/s12206-007-1018-5.
[21] M.Y. Khan, Z.A.A. Karim, A.R.A. Aziz, I.M. Tan, A case study on the influence of selected parameters on microexplosion behavior of water in biodiesel emulsion droplets, J. Energy Resour. Technol. 139 (2) (2017), 022203 (10 pages), https://doi.org/10.1115/1.4034230.
[22] V.M. Ivanov, P.I. Nefedov, Experimental investigation of the combustion process of natural and emulsified liquid fuels, NASA TT F-258, 1965.
[23] O.G. Girin, Dynamics of the emulsified fuel droplet micro-explosion, Atom. Sprays 27 (2017) 407–422.
[24] Y. Zhang, Y. Huang, R. Huang, S. Huang, Y. Ma, S. Xu, Z. Wang, A new puffing model for a droplet of butanol-hexadecane blends, Appl. Therm. Eng. 133 (2018) 633–644.
[25] C.T. Avedisian, I. Glassmann, Superheating and boiling of water in hydrocarbons at high pressures, Int. J. Heat Mass Transfer 24 (1981) 695–706.
[26] H.S. Carslaw, J.C. Jaeger, Conduction of Heat in Solids, Clarendon Press, Oxford, 1986.
[27] E.M. Kartashov, Analytical Methods in the Heat Transfer Theory in Solids. Vysshaya Shkola, Moscow (in Russian), 2001.
[28] S.S. Sazhin, Droplets and Sprays, Springer, 2014.
[29] S.S. Sazhin, P.A. Krutitskii, S.B. Martynov, D. Mason, M.R. Heikal, E.M. Sazhina, Transient heating of a semitransparent spherical body, Int. J. Therm. Sci. 46 (2007) 444–457.
[30] S.S. Sazhin, I.G. Gusev, P.A. Krutitskii, M.R. Heikal, Transient heating of a semitransparent spherical body immersed into a gas with inhomogeneous temperature distribution, Int. J. Therm. Sci. 50 (2011) 1215–1222.
[31] M.A. Ismael, M.R. Heikal, A.R. Aziz, C. Crua, M. El-Adawy, Z. Nissar, M.B. Baharom, E.Z. Zainal A, F. Syah, Investigation of puffing and micro-explosion of water-in-diesel emulsion spray using shadow imaging, Energies 11 (9) (2018) 2281.